THE JOURNAL OF PHYSICAL CHEMISTRY Letters

Letter

pubs.acs.org/JPCL

Direct Dynamics Studies of a Binuclear Metal Complex in Solution: The Interplay Between Vibrational Relaxation, Coherence, and Solvent Effects

Asmus Ougaard Dohn,*[,†] Elvar Örn Jónsson,[‡] Kasper Skov Kjær,[‡] Tim Brandt van Driel,[‡] Martin Meedom Nielsen,[‡] Karsten Wedel Jacobsen,[‡] Niels Engholm Henriksen,[†] and Klaus Braagaard Møller*[,†]

[†]Department of Chemistry, Technical University of Denmark, Building 207, 2800 Kongens Lyngby, Denmark

[‡]Department of Physics, Technical University of Denmark, Building 307, 2800 Kongens Lyngby, Denmark

Supporting Information

ABSTRACT: By using a newly implemented QM/MM multiscale MD method to simulate the excited state dynamics of the $Ir_2(dimen)_4^{2+}$ (dimen = 1,8-diisocyano-*p*-menthane) complex, we not only report on results that support the two experimentally observed coherent dynamical modes in the molecule but also reveal a third mode, not distinguishable by spectroscopic methods. We directly follow the channels of energy dissipation to the solvent and report that the main cause for coherence decay is the initial wide range of configurations in the excited state population. We observe that the solvent can actually extend the coherence lifetime by blocking channels for intramolecular vibrational energy redistribution (IVR).

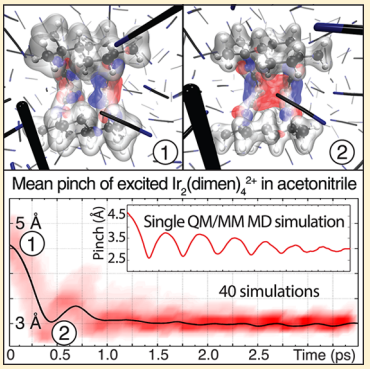

SECTION: Spectroscopy, Photochemistry, and Excited States

One way of exploring the dynamical nature of chemical reactions has been facilitated through the study of bimetallic d^8–d^8 complexes and their remarkable photochemical properties[1−7] since their first synthesis almost four decades ago.[5] The focus of this work is on $Ir_2(dimen)_4^{2+}$ (dimen = 1,8-diisocyano-*p*-menthane), a type of molecule that has also shown photoconversion functionality for solar energy storage.[4] Systems of this type are also uniquely relevant in ultrafast time-resolved X-ray experiments.[8−16]

The electronic configuration of this complex features a σ antibonding highest occupied molecular orbital (HOMO), whereas the lowest unoccupied molecular orbital (LUMO) is σ bonding (Figure 1).[1,2] This causes the complex to undergo large structural changes when photoexcited.[17−19] Our group observed a contraction of the metal−metal distance in the Ir variant in solution by 1.4 Å,[19] using ∼100 ps pulsed synchrotron radiation. We have recently gathered data on this system at the Linac Coherent Light Source (LCLS) to directly probe the coherent motion with X-ray methods, utilizing the higher temporal resolution of X-ray free electron lasers, compared with synchrotron radiation. Analysis is ongoing.

Hartsock et al.[3] have carried out transient spectroscopy measurements on the $Ir_2(dimen)_4^{2+}$ complex, and report a deformational isomerism which effectively splits the ground state (GS) population in two main structures: a "short and twisted" (Ir−Ir distance of ∼3.6 Å, 17° twist), and a "long and eclipsed" (Ir−Ir distance of ∼4.4 Å, 0° twist). This isomerism has previously been observed[6] and is supported computationally by constrained mappings of the GS energy landscape.[20] However, to our knowledge, no attempts (including our own) to freely relax the geometry of the molecule into the short conformer has proved successful when using DFT methods, and therefore, this study is focused only on the long and eclipsed conformer. For this conformer, Hartsock et al. observe oscillations in the transient absorption with a frequency of 75 cm^{-1} occurring 0.5 ps after excitation, which they assign to wavepacket motion in the previously mentioned metal−metal contraction on S_1, whose lifetime is determined to ∼65 ps.[19]

With this work, we aim to expand on the pre-existing knowledge about the system using our newly developed QM/MM Born−Oppenheimer MD (QM/MM BOMD) method[21] to obtain an adiabatic version of the vibrational motion in the single molecule. By utilizing the efficiency of the code, we mimic the coherent motion by exciting a host of different GS configurations and analyze the mean properties of these dynamic trajectories and their relation to individual excitations. By benchmarking these results against experiments, we obtain information not experimentally distinguishable, such as possible

Received: April 30, 2014
Accepted: June 23, 2014
Published: June 23, 2014

   dx.doi.org/10.1021/jz500850s | *J. Phys. Chem. Lett.* 2014, 5, 2414−2418

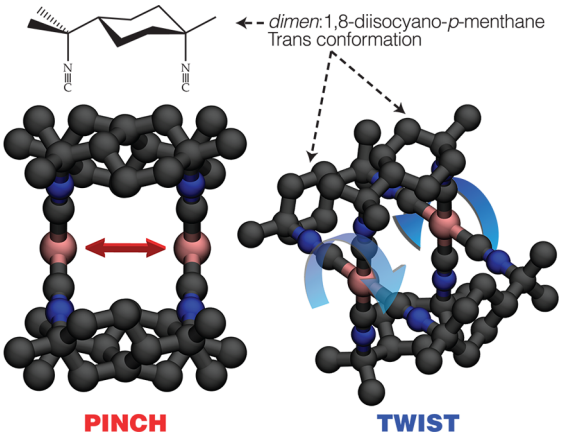

Figure 1. Two of the main dynamic, structural modes of $Ir_2(dimen)_4^{2+}$, shown here without hydrogens for clarity, for the conformer employed in this study (see text for discussion of GS conformers). The 1,8-diisocyano-*p*-menthane (dimen) ligand provides the optimal compromise between flexibility and rigidity for large, but controllable structural changes, for example, by electronic excitation. Electronically exciting this complex promotes an electron from the antibonding HOMO to the bonding LUMO, effectively forming a chemical bond between the Ir atoms[1−3]

Figure 2 shows the GS trajectory from which 40 configurations are excited, for a total of 140 ps ES trajectories

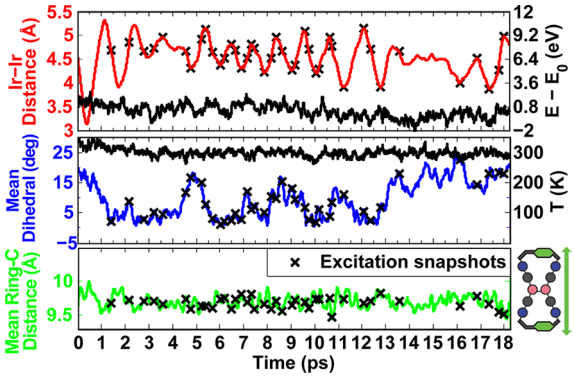

Figure 2. Structural modes in $Ir_2(dimen)_4^{2+}$ plotted for the GS trajectory. Top: Ir−Ir distance. Middle: Mean dihedral angle. The black graphs show the total energy difference during the run (where E_0 is the total energy at the start of the production run) and temperature in the top and middle graph, respectively. Bottom: Mean distance between opposite carbon atoms in the ligand rings. This parameter describes a breathing motion which will play an important role in the excited state (see text). The ES runs were started from the configurations marked with black crosses.

dynamics of spectroscopically dark or obscured modes, direct observation of intra- and intermolecular energy transfer and solvent interactions. Since the electronic structure of the QM part is calculated "on the fly", and no full potential energy surfaces (PESes) are calculated (or needed) in this direct-dynamics method, we focus on simulating the structural dynamics upon excitation of a population of solvated $Ir_2(dimen)_4^{2+}$ from the long GS conformer. The Direct-Dynamics simulations were carried out utilizing the Atomic Simulation Environment (ASE)[22] to interface the QM and MM subsystems. The grid-based projector-augmented wave method (GPAW)[23] is used for the QM description. The full details of the method and its interfacing strategy is described elsewhere.[21] The quantum system comprised of the $Ir_2(dimen)_4^{2+}$ complex is described using DFT with the PBE functional.[24] It was placed in a classically prethermalized simulation box of 28 × 28.5 × 31.5 Å containing acetonitrile at 0.786 g/cm^3. After removal of acetonitrile molecules overlapping with the complex, the total number of classically described acetonitriles was 237. The entire system was then thermalized again, until the temperature was stable at 300 K, as set by the Langevin thermostat applied to the solvent only. For the production run, 18.21 ps of GS trajectory was sampled using 2 fs timesteps.

We approximate the experimental excitation by instantaneously promoting a comprehensive representation of the GS configuration space to the excited state (ES), neglecting effects from finite pulse-widths and bandwidths of real excitation sources (the effect of the bandwidth is examined in the Supporting Information).[25] The ultrafast ES dynamics is believed to take place on S_1, but because similar binuclear d^8−d^8 complexes have previously been shown to have the same triplet and singlet surface shapes, only differing in energy,[15,26] it is assumed possible to carry out T_1 simulations mimicking the ES S_1 dynamics. Thus, the computational cost is kept within the feasible range for systems of this size by staying within the GS DFT framework on T_1. This approximation is implied for all the excitations simulated in this work.

sampled. The sampling was spaced such as to minimize the correlation between each of the ES trajectories while also allowing for comparison of excitations from complexes of similar starting geometries, but with different solvent configurations, and excitations from different starting geometries. The thermostat was turned completely off for these runs. The ES time step was 1 fs, to allow better resolution and minimize the drift. The maximum observed drift in any of the simulations was 0.40 kJ/mol per atom in the system, over the entire simulation duration.

Figure 3 shows three modes: pinch, twist, and breathing (definitions given in the caption). The mean Ir−Ir distance in the population when measured over the last picosecond of the simulation is 2.98 Å, which is in very good agreement with previous experimental results from X-ray scattering[19] of 2.90 Å. The second inset in the top figure shows that the pinching motion is limited to the center part of the molecule, affecting the next two atoms adjacent to Ir, but not the outermost parts of the ligands. The mean values of the entire population show oscillatory features, meaning that the motion of each trajectory is in phase with the others, thus showing signs of coherent motion. The excited population loses its mean pinch oscillation amplitude almost before completing a full period, but if the first oscillation period is calculated by doubling the time from the first well to the first top, the period is ∼480 fs, or ∼70 cm^{-1}.

The frequency differs only 7% from the experimentally observed frequency of 75 cm^{-1}.[3] This agreement further validates the assumption of very similar S_1 and T_1 PES shapes.

The anharmonicity of the underlying potential, is evident in the direct dynamics from the oscillation in the single trajectory (top inset in Figure 3): it reflects a steeper potential for the short distances and a gentler slope for the long ones. The oscillation becomes more sinusoidal with time, as the trajectory moves closer to the harmonic approximation limit, deeper in the potential. Similarly, the frequency increases as the molecule dissipates its excess vibrational energy (also observed for the single trajectory), which is equivalent to anharmonic potentials

dx.doi.org/10.1021/jz500850s | J. Phys. Chem. Lett. 2014, 5, 2414−2418

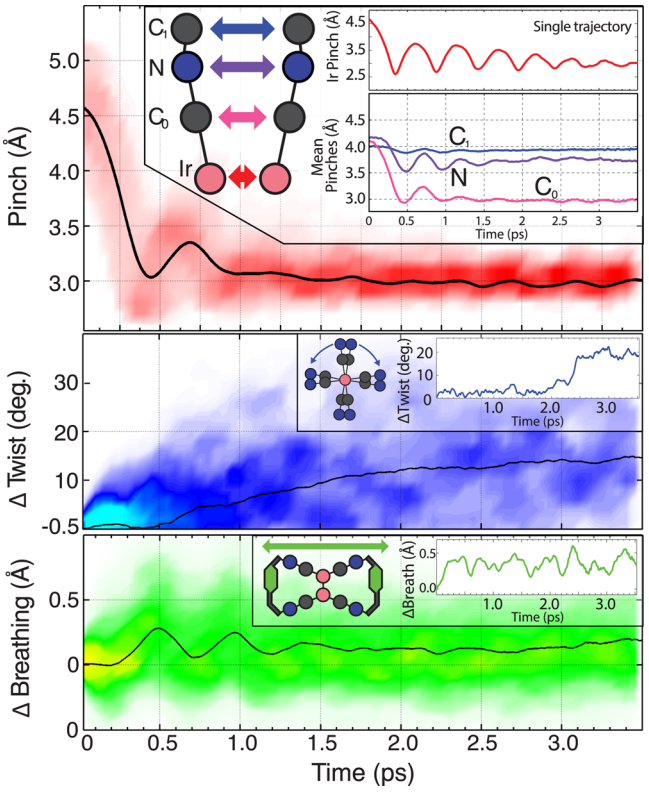

Figure 3. Ir–Ir pinching (top), twisting (middle), and breathing (bottom) as a function of time after excitation. The twist and the breathing is defined as the change in mean dihedral angle and in mean distance between opposite ring-carbons in the ligands, respectively, from the moment of excitation. The black curves are the averages, whereas the shaded backgrounds show the binned counts of values from all trajectories. The bin sizes are 50 fs by 0.1 Å, 0.05 Å, and 2 degrees for the pinching, breathing, and twisting, respectively. This population loses its pinch phase within a picosecond, whereas the single trajectory-pinch oscillation dies out much slower, as can be seen on the top inset. However, the mean phase of the breathing mode is sustained for almost 1.5 ps. The pinching and breathing modes share the same oscillation period . The next inset on the top graph shows that the two atoms in each ligand closest to Ir are also pinching, whereas the next carbon (C_1) is almost unaffected.

with Morse-like characteristics. Because the experimental frequency is first measured at times $t \geq 0.5$ ps after excitation (when the molecule has already dissipated some of the excess energy), it is expected that our first simulated oscillation period is longer than the experimental result. Also consistent with experimental results,[3] little to no coherent twist oscillation is observed from excitations that start from the long, eclipsed conformation. However, a delayed twist mechanism is observed for the mean motion, with the molecule starting to twist after roughly 500 fs. The delayed onset of both twisting and breathing indicates that the modes are activated by the pinching of the Ir atoms.

The simulation coherence decay is faster than the experimental one if only the pinch is taken into account. However, the breathing mode is coherent for almost 1.5 ps. Furthermore, the frequency of the pinching and breathing is similar: The period from the first to the second top is ~450 fs, or ~74 cm^{-1}, only 1.3% slower than the experimental pinch. We note that the ES breathing amplitude in individual trajectories can be roughly 4 times larger than the amplitude of the GS trajectory shown in Figure 2.

The causes of coherence decay can be either statistical or dynamical in nature, that is, either a result of the difference in initial configurations from which the system is brought up to the excited state, or due to (stochastic) energy dissipation in each molecule, either through the solvent or through internal degrees of freedom. Examinations of the individual trajectories (Figure 3, top inset) reveal that vibrational relaxation is much slower than the population mean coherence decay and not very stochastic in nature. Hence, the fast coherence decay of the population mean must originate from the wide range of initial GS configurations. This is supported by a thorough population-partitioning analysis (see Supporting Information for details), which shows that exciting a narrow, phase-coherent distribution of GS configurations extends the coherence time on the excited state significantly. Our analysis also shows that introduction of an effective bandwidth in making the ES population, similar to the one of the experimental excitation source,[3] leads to a somewhat longer excited-state coherence time, although there is no strong correlation between the GS metal–metal vibrational amplitude/phase and the excitation energy.

In order to further understand the effect of the solvent on $Ir_2(dimen)_4^{2+}$ dynamics, Figure 4 compares the pinch of the

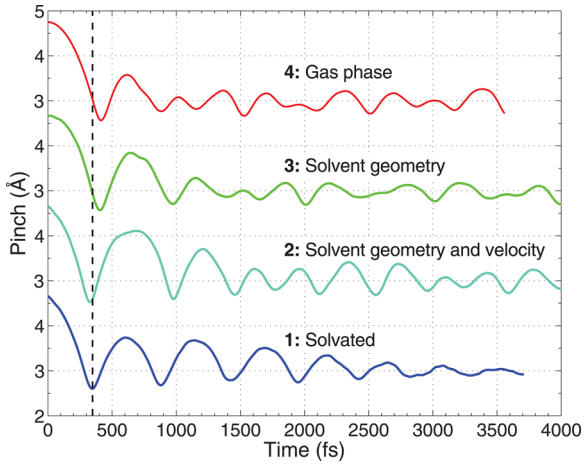

Figure 4. In order to investigate the role of the solvent in the dynamics, three other ES trajectories were also simulated, and shown here, together with a single trajectory from the main production run. **1:** The pinch of the fully solvated complex. **2:** A simulation where the solvent was removed at the time of excitation, but keeping the initial geometry influenced by the solvent *and* the velocity of the atoms in the complex. **3:** A simulation where only the geometry is kept while the initial velocities are set to zero. **4:** An excitation started from the gas phase, zero kelvin structure of the complex.

single trajectory from the inset of Figure 3 to a group of additional simulations that have progressively more gas-phase character (from bottom to top in the figure).

The first noticeable feature is the fast quenching of Ir–Ir oscillations in **4**, indicating efficient intramolecular vibrational energy redistribution (IVR) in the pure gas phase simulation, which is evidently the *only* possible channel for energy redistribution in that system. In this case, the excess vibrational energy is efficiently transferred away from the pinch. The original trajectory (**1**) was excited from a GS phase space area of already contracting metal atoms, which explains why the first contraction of the metal atoms in simulations **1** and **2** is faster than in **3** and **4**. The second contraction is fastest in **1**, and the amplitude of the pinching motion is the smallest, consistent

dx.doi.org/10.1021/jz500850s | J. Phys. Chem. Lett. 2014, 5, 2414–2418

with anharmonic oscillation, damped by the solvent. However, at longer times, the solvent cage apparently *facilitates* the oscillatory nature of the pinching motion in **1**, compared to the other trajectories.

Figure 5 analyzes the interplay between IVR and solvation. In trajectory 1 on Figure 5, the pinch energy is redistributed

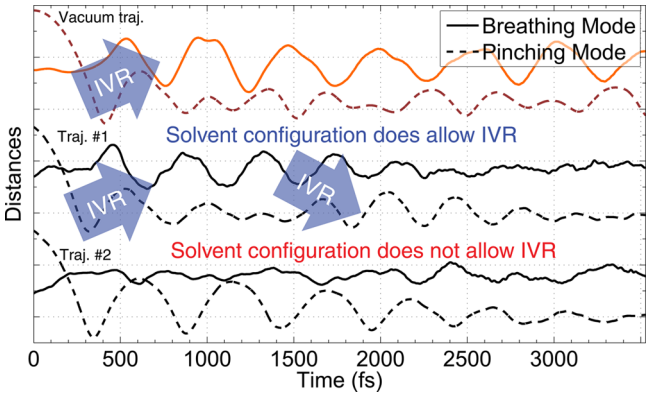

Figure 5. Comparison of the breathing mode in the gas phase trajectory (red) and two trajectories of solvated systems, displaying the energy transfer mechanisms in the system. The two solvent-included trajectories are started from similar GS conditions, but 10 ps apart, so the two accompanying solvent configurations are uncorrelated. The breathing mode amplitude is large in gas phase, compared to the other trajectories, because there is no dampening from the solvent. The small perturbations in the breathing oscillation is attributed to solute−solvent interactions, governing the vibrational relaxation through the solvent.

almost completely to the breathing mode within 1.5 ps, where solvent-induced interactions perturb the oscillation. Some of the remaining energy is then again transferred back into the pinch before dissipating further. In trajectory 2, the solvent configuration apparently does not allow for IVR to the breathing mode, so the excess excitation energy is contained in the pinch, which has almost none of the smaller perturbations stemming from interactions with the solvent. All in all, this means that vibrational relaxation of $Ir_2(dimen)_4^{2+}$ at early times is substantially mediated by IVR into the breathing mode and that, in some instances, the solvent may hinder this motion, which in turn extends the coherence time of the pinch compared to vacuum.

That the coherence decay is faster than vibrational cooling is in contrast with the findings of van der Veen et al.[15] for the bimetallic d^8-d^8 complex $[Pt_2(P_2O_5H_2)_4]^{4-}$ in various solvents, where the authors observe that coherence decay occurs on the same time scale as vibrational cooling. Although the two complexes are different, and different solvents are used (including protic solvents), they both have coordination sites along the metal atom axis, which could facilitate significant electrostatic and dispersion interactions with the solvent. Nevertheless, the main difference causing the contrasting results is most likely due to the different rigidities of the two distinct ligand types, where the more flexible dimen ligand allows for a wider range of configurations in the GS ensemble. We emphasize that here, the variation of the GS metal−metal distance (Figure 2) is comparable to the amplitude of the excited state vibration (Figure 3).

Both the $Ir_2(dimen)_4^{2+}$ and $[Pt_2(P_2O_5H_2)_4]^{4-}$ experiments represent the formation of a chemical bond in a "scaffolded diatomic". Recently, we have investigated the solvent-induced bond formation in a true diatomic molecule: the ground-state recombination of I_2, following photoinduced dissociation.[27] In this system, we observed the same behavior as for $Ir_2(dimen)_4^{2+}$: the coherence decay is much faster than vibrational cooling. However, because I_2 is bound in the ground state, the original GS distribution is very narrow, compared to amplitude of the motion following photo excitation, and it is therefore not a source of decoherence. The cause of I_2 decoherence is still statistical: it is due to the direct interaction with its solvent cage, which lacks in both the order and rigidity compared to the molecular scaffold of the bimetallic complexes.

In conclusion, this work demonstrates that the implementation using GPAW for the QM description in this multiscale method is capable of producing out-of-equilibrium molecular dynamics with statistical quantities that make it possible to obtain information on the mean dynamics of populations. The experimental Ir−Ir pinch and twist dynamics are reproduced. We observed a previously undiscovered (to our knowledge) breathing mode. This mode stays coherent for longer time than the pinch and is apparently the first recipient of the excess energy transferred out of the pinch mode. We note that in some configurations, the rigidity of the solvent cage can block the breathing motion and thereby sustain the coherence of the pinch mode.

By looking at the shapes of the individual trajectories, we have argued that the major electrostatic solute−solvent interaction occurs through the ligands for this complex and that the IVR here is delayed because the metals need to contract first. At last, the breathing occurs in the ligands and is perpendicular to the pinch axis. As such, the (rigidity of the) ligands play an important role in the complex, both through defining the width of the GS ensemble, which affects the ES population coherence, and as mediators of the solvent interaction.

■ ASSOCIATED CONTENT

Ⓢ Supporting Information

Supplies background to the simulations and includes an analysis of the ES population. It also includes a video showing the breathing mode for the vacuum trajectory.This material is available free of charge via the Internet at http://pubs.acs.org/.

■ AUTHOR INFORMATION

Corresponding Authors

*A. O. Dohn. E-mail: asod@kemi.dtu.dk.
*K. B. Møller. E-mail: klaus.moller@kemi.dtu.dk.

Notes

The authors declare no competing financial interest.

■ ACKNOWLEDGMENTS

The authors thank Robert W. Hartsock, Kelly Gaffney, & Kristoffer Haldrup for discussion and feedback. This work was funded by the Lundbeck Foundation and the Danish National Research Foundation's Centre for Molecular Movies.

■ REFERENCES

(1) Mann, K. R.; Gordon, J. G. I.; Gray, H. B. Characterization of Oligomers of Tetrakis(Phenyl Isocyanide)Rhodium(I) in Acetonitrile Solution. *J. Am. Chem. Soc.* **1975**, *97*, 3553−3555.
(2) Roundhill, M. D.; Gray, H. B.; Che, C. Pyrophosphito-Bridged Diplatinum Chemistry. *Acc. Chem. Res.* **1989**, *22*, 55−61.
(3) Hartsock, R. W.; Zhang, W.; Hill, M. G.; Sabat, B.; Gaffney, K. J. Characterizing the Deformational Isomers of Bimetallic $Ir_2(dimen)_4^{2+}$

(dimen= 1,8-diisocyno-*p*-menthane) with Vibrational Wavepacket Dynamics. *J. Phys. Chem. A* **2011**, *115*, 2920.
(4) Mann, K. R.; Lewis, N. S.; Miskowski, V. M.; Erwin, D. K.; Hammond, G. S.; Gray, H. B. Solar-Energy Storage - Production of Hydrogen by 546-nm Irradiation of a Dinuclear Rhodium(ii) Complex in Acidic Aqueous-Solution. *J. Am. Chem. Soc.* **1977**, *99*, 5525−5526.
(5) Lewis, N. S.; Mann, K. R.; Gordon, J. G.; Gray, H. B. Oligomerization and 2-Center Oxidative Addition-Reactions of a Dimeric Rhodium(II) Complex. *J. Am. Chem. Soc.* **1976**, *98*, 7461−7463.
(6) Exstrom, C. L.; Britton, D.; Mann, K. R. Structures of $[M_2(dimen)_4](Y)_2$ (M = Rh, Ir; dimen = 1,8-Diisocyanomenthane; Y = PF6, Tetrakis[3,5-bis(Trifluoromethyl)Phenyl]Borate, $B(C_6H_5)_4$) Crystals Featuring an Exceptionally Wide Range of Metal-Metal Distances and Dihedral Twist Angles. *Inorg. Chem.* **1996**, *35*, 549−550.
(7) Harvey, P. D.; Murtaza, Z. Properties of Pd^1-Pd^1 Bonds - Theoretical and Spectroscopic Study of Pd_2(dmb)2 × 2 Complexes (Dmb = 1,8-Diisocyano-P-Menthane, X = Cl,br). *Inorg. Chem.* **1993**, *32*, 4721−4729.
(8) Møller, K. B.; Henriksen, N. E. Time-Resolved X-Ray Diffraction: The Dynamics of the Chemical Bond. *Struct. Bonding (Berlin)* **2012**, *142*, 185−212.
(9) Haldrup, K.; Christensen, M.; Cammarata, M.; Kong, Q.; Wulff, M.; Mariager, S. O.; Bechgaard, K.; Feidenhans'l, R.; Harrit, N.; Nielsen, M. M. Structural Tracking of a Bimolecular Reaction in Solution by Time-Resolved X-Ray Scattering. *Angew. Chem.* **2009**, *48*, 4180−4184.
(10) van der Veen, R. M.; Milne, C. J.; Nahas, A. E.; Lima, F. A.; Van-Thai, P.; Best, J.; Weinstein, J. A.; Borca, C. N.; Abela, R.; Bressler, C.; et al. Structural Determination of a Photochemically Active Diplatinum Molecule by Time-Resolved EXAFS Spectroscopy. *Angew. Chem.* **2009**, *48*, 2711−2714.
(11) Christensen, M.; Haldrup, K.; Kjær, K. S.; Cammarata, M.; Wulff, M.; Bechgaard, K.; Weihe, H.; Harrit, N.; Nielsen, M. M. Structure of a Short-Lived Excited State Trinuclear Ag-Pt-Pt Complex in Aqueous Solution by Time Resolved X-ray Scattering. *Phys. Chem. Chem. Phys.* **2010**, *12*, 6921−6923.
(12) van der Veen, R. M.; Kas, J. J.; Milne, C. J.; Van-Thai, P.; El Nahhas, A.; Lima, F. A.; Vithanage, D. A.; Rehr, J. J.; Abela, R.; Chergui, M. L-edge XANES analysis of photoexcited metal complexes in solution. *Phys. Chem. Chem. Phys.* **2010**, *12*, 5551−5561.
(13) Christensen, M.; Haldrup, K.; Bechgaard, K.; Feidenhans'l, R.; Kong, Q.; Cammarata, M.; Russo, M. L.; Wulff, M.; Harrit, N.; Nielsen, M. M. Time-Resolved X-ray Scattering of an Electronically Excited State in Solution. Structure of the $^3A_{2u}$ State of Tetrakis-μ-pyrophosphitodiplatinate(II). *J. Am. Chem. Soc.* **2011**, *131*, 502−508.
(14) Kong, Q.; Kjær, K. S.; Haldrup, K.; Sauer, S. P. A.; van Driel, T. B.; Christensen, M.; Nielsen, M. M.; Wulff, M. Theoretical Study of the Triplet Excited State of PtPOP and the Exciplexes M-PtPOP (M = Tl, Ag) in Solution and Comparison with Ultrafast X-ray Scattering Results. *Chem. Phys.* **2012**, *393*, 117−122.
(15) van der Veen, R. M.; Cannizzo, A.; van Mourik, F.; Vlcek, A. J.; Chergui, M. Vibrational Relaxation and Intersystem Crossing of Binuclear Metal Complexes in Solution. *J. Am. Chem. Soc.* **2011**, *113*, 305.
(16) Penfold, T. J.; Curchod, B. F. E.; Tavernelli, I.; Abela, R.; Rothlisberger, U.; Chergui, M. Simulations of X-Ray Absorption Spectra: The Effect of the Solvent. *Phys. Chem. Chem. Phys.* **2012**, *14*, 9444−9450.
(17) Miskowski, V. M.; Rice, S. F.; Gray, H. B. Spectroscopy and Photophysics of $Rh_2(dimen)_4^{2+}$ (Dimen = 1,8-Diisocyanomenthane). Exceptional Metal-Metal Bond Shortening in the Lowest Electronic Excited States. *Inorg. Chem.* **1994**, *33*, 2799−2807.
(18) Coppens, P.; Gerlits, O.; Vorontsov, I. I.; Kovalevsky, A.; Chen, Y.; Graber, T.; Gembicky, M.; Novozhilova, I. A Very Large Rh-Rh Bond Shortening on Excitation of the $[Rh_2$ (1,8-Diisocyano-*p*-Mentane)$_4]^{2+}$ ion by Time-Resolved Synchrotron X-Ray Diffraction. *Chem. Commun.* **2004**, *19*, 2144−2145.
(19) Haldrup, K.; Harlang, T.; Christensen, M.; Dohn, A.; van Driel, T. B.; Kjær, K. S.; Harrit, N.; Vibenholt, J.; Guerin, L.; Wulff, M.; et al. Bond Shortening (1.4 Å) in the Singlet and Triplet Excited States of $[Ir_2(dimen_4]^{2+}$ in Solution Determined by Time-Resolved X-Ray Scattering. *Inorg. Chem.* **2011**, *50*, 9329.
(20) Hunter, B. M.; Villahermosa, R. M.; Exstrom, C. L.; Hill, M. G.; Mann, K. R.; Gray, H. B. M-M Bond-Stretching Energy Landscapes for $M_2(dimen)_4^{2+}$ (M = Rh, Ir; dimen = 1,8-Diisocyanomenthane) Complexes. *Inorg. Chem.* **2012**, *51*, 6898−6905.
(21) Jónsson, E. O.; Thygesen, K. S.; Ulstrup, J.; Jacobsen, K. W. *Computational Approach to Electron Charge Transfer Reactions*; Technical University of Denmark: Lyngby, Denmark, 2014.
(22) Bahn, S. R.; Jacobsen, K. W. An Object-Oriented Scripting Interface to a Legacy Electronic Structure Code. *Comput. Sci. Eng.* **2002**, *4*, 55.
(23) Mortensen, J. J.; Hansen, L. B.; Jacobsen, K. W. Real-Space Grid Implementation of the Projector Augmented Wave Method. *Phys. Rev. B* **2005**, *71*, 035109.
(24) Perdew, J. P.; Burke, K.; Ernzerhof, M. Generalized Gradient Approximation Made Simple. *Phys. Rev. Lett.* **1996**, *77*, 3865−3868.
(25) Petersen, J.; Henriksen, N. E.; Møller, K. B. Validity of the Bersohn−Zewail Model Beyond Justification. *Chem. Phys. Lett.* **2012**, *539*−*540*, 234−238.
(26) Stiegman, A. E.; Rice, S. F.; Gray, H. B.; Miskowski, V. M. Electronic Spectroscopy of d^8-d^8 Diplatinum Complexes. $^1A_{2u}(d\sigma^* \rightarrow p\sigma)$, $^3E_u(d_{xz},d_{yz} \rightarrow p\sigma)$, and $^{3,1}B_{2u}(d\sigma^* \rightarrow d_{x^2-y^2}$ Excited States of $Pt_2(P_2O_5H_2)_2^{4-}$. *Inorg. Chem.* **1987**, *26*, 1112.
(27) Lee, J. H.; Wulff, M.; Bratos, S.; Petersen, J.; Guerin, L.; Leicknam, J. C.; Cammarata, M.; Kong, Q.; Kim, J.; Møller, K. B.; Ihee, H. Filming the Birth of Molecules and Accompanying Solvent Rearrangement. *J. Am. Chem. Soc.* **2013**, *135*, 3255−3261.

Direct Dynamics Studies of a Binuclear Metal Complex in Solution: The Interplay Between Vibrational Relaxation, Coherence, and Solvent Effects. Supporting Info

Asmus Ougaard Dohn,*,† Elvar Örn Jónsson,‡ Kasper Skov Kjær,‡ Tim Brandt van Driel,‡ Martin Meedom Nielsen,‡ Karsten Wedel Jacobsen,‡ Niels Engholm Henriksen,† and Klaus Braagaard Møller†

Department of Chemistry, Technical University of Denmark, Building 207, 2800 Kgs. Lyngby, Denmark, and Department of Physics, Technical University of Denmark, Building 307 2800 Kgs. Lyngby, Denmark

E-mail: asod@kemi.dtu.dk

*To whom correspondence should be addressed
†DTU Chemistry
‡DTU Physics

SI: Further Computational Details

The QM/MM MD simulations were made using the QM/MM Scheme presented in[1], which interfaces the two regions through the total energy of the system:

$$E_{\mathrm{tot}} = E_{\mathrm{QM}} + E_{\mathrm{MM}} + E_{\mathrm{QM/MM}} \tag{1}$$

where the three terms represent the energy of the QM subsystem, the MM subsystem and their interaction energy, respectively. The interaction energy consists of a Coulomb term between the electronic density and the classical point charges, a Coulomb term between the nuclei in the QM subsystem and the MM point charges, and a Lennard-Jones (LJ) term:

$$E_{\mathrm{QM/MM}} = \sum_{i}^{N_{\mathrm{MM}}} q_i \int \frac{n(\mathbf{r})}{|\mathbf{r} - \mathbf{R}_i|} d\mathbf{r} + \sum_{i}^{N_{\mathrm{MM}}} \sum_{\alpha}^{N_{\mathrm{QM}}} \frac{q_i Z_\alpha}{|\mathbf{R}_\alpha - \mathbf{R}_i|} + E_{\mathrm{LJ}} \tag{2}$$

$$E_{\mathrm{LJ}} = \sum_{i}^{N_{\mathrm{MM}}} \sum_{\alpha}^{N_{\mathrm{QM}}} 4\epsilon_{i\alpha} \left[\left(\frac{\sigma_{i\alpha}}{|\mathbf{R}_\alpha - \mathbf{R}_i|} \right)^{12} - \left(\frac{\sigma_{i\alpha}}{|\mathbf{R}_\alpha - \mathbf{R}_i|} \right)^{6} \right] \tag{3}$$

The LJ parameters are combined using the Waldman-Hagler rule.[2]

The first term in eqn. 1 is evaluated with density functional theory (DFT), using the grid-based projector augmented wave method, implemented in the GPAW package,[3] which is modified so that the total effective potential also contains a term from the MM subsystem. The calculations were performed with a localised atomic orbital basis in combination with the real space grid, allowing for high parallelisation as well as fast diagonalization of the principal matrices.

Preliminary Tests

Preliminary calculations showed that a simulation box with 4 Å of vacuum padding in each dimension was enough to fully eliminate effects from truncating the wave functions, so the cell size for each simulation (both GS and ES) was chosen thusly. Test geometry

calculations were performed in vacuum, and the results are shown in fig. 1. The max Ir-Ir

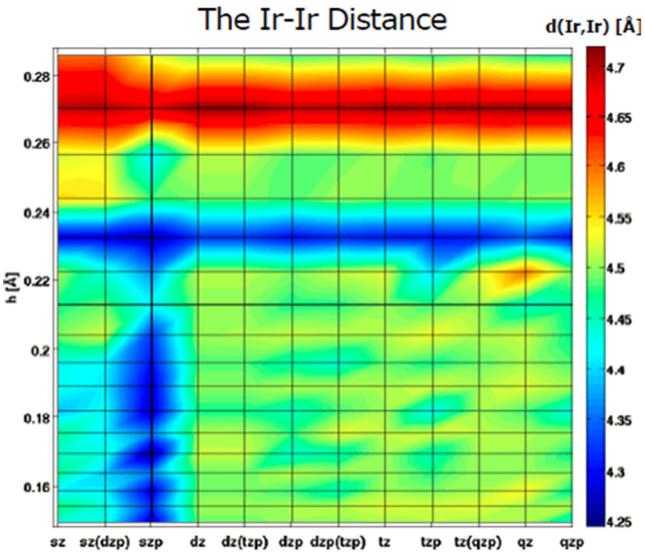

Figure 1: Convergence of the main structural parameter of the complex - the Ir-Ir distance - with respect to the real space grid spacing h, and size of basis set. A stable value for the distance is maintained when employing values of $h < 0.22$ Å with basis sets of at least double-zeta size. The convergence criteria for each individual relaxation was a maximum force of 0.05 eV / Å on any of the atoms in the system.

distance difference in the grid spacing region $0.15 \leq h \leq 0.21$ is less than 3.5 % of the largest distance, so instead of fixing the grid spacing to a definite value, it was possible to speed up the simulation even further by keeping the number of grid points to values divisible by eight, i.e. (112,120,112) for the (x,y,z) dimensions. Since the overall size of the molecule varies for each of the initial GS configurations used in the the ES simulations, so does the QM cell, resulting in grid spacings $0.1571 \leq h \leq 0.1931$, well within the converged region shown in fig. 1. The basis set used was of tzp quality for Ir and dzp for the rest of the molecule. The chosen PBE vacuum description overshoots the Ir-Ir distance (as does the mean QM/MM value), when compared to the experimental value of the solvated complex:[4] 4.3 Å. Crystalline values range from 3.601 Å to 4.414 Å, depending on the type of counter ion.[5]

The Acetonitrile solvent

Since the predominantly used solvent for $Ir_2(dimen)_4^{2+}$ is Acetonitrile (ACN), a classical, rigid, 3-point interaction potential was adapted from Guardia *et al.*[6] A simulation box of 28x28.5x31.5 Å was filled with 290 ACN molecules and thermalized. An MM production run of 0.5 ns was used to obtain radial distribution functions (RDFs). In order to also confirm a proper QM/MM interfacing, RDFs between a single QM ACN and the remaining MM ACNs were produced, and compared to RDFs obtained only using MM MD. Parallel QM/MM runs with a single QM ACN were branched off the production MM trajectory, insterspaced by 500 fs, to avoid any correlation between the new trajectories (see the velocity autocorrelation function inset on fig. 2). A Langevin-type thermostat was used in both the MM and QM/MM runs, with a friction coefficient of 0.05 and 2 fs timesteps. The hydrogens on the QM were constrained using the RATTLE scheme.[7] Each QM/MM trajectory was thermalized again, before sampling the RDFs. A total of 0.5 ns and 0.25 ns of dynamics were sampled for the MM and QM/MM systems, respectively. There is generally a good agreement between the various descriptions. The literature RDFs[6] have been produced in the NPT ensemble, which might be the cause of some of the small differences. Furthermore, the electronic structure description used to create the force field is not the same as the one used in the QM/MM simulations, and the force field is not optimized to work in a QM/MM framework.

Further ES population analysis

In principle, an instantaneous excitation corresponds to an infinite bandwidth. However, a more realistic representation of an experiment can be obtained by including an effective, finite bandwidth[8]. This can be included by estimating the effective bandwidth of our range of ES simulations in fig. 3, and compare the pinch oscillation from different, relevant subsets with similar sampling statistics of the entire ES population in fig. 4, to elucidate how this affects the coherence lifetime.

The simplest way to approximate the excitation energy is simply to subtract a single point

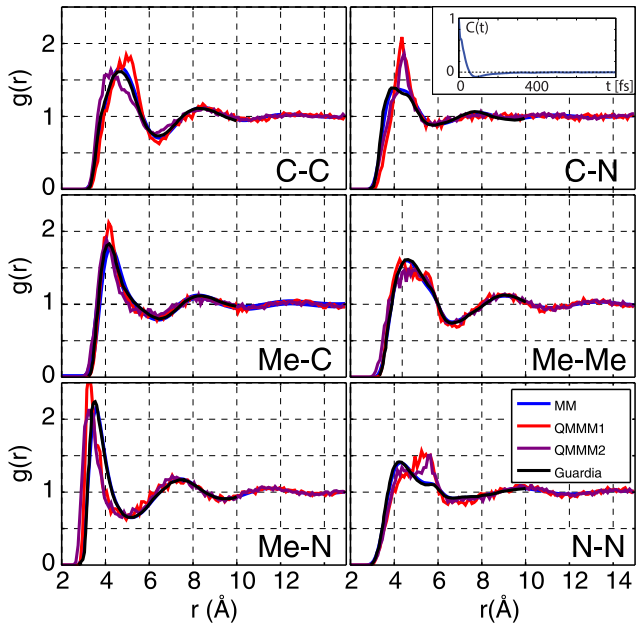

Figure 2: Radial distribution functions (RDFs) of the 6 intermolecular distances of ACN. The RDFs are calculated every 500th fs in trajectories of 0.5 ns and 0.25 ns for the MM and QM/MM systems, respectively. The QM/MM systems are comprised of a single QM ACN in a bath of MM ACN. The QM/MM1 systems are made using methyl-group vdW parameters for the middle Carbon, while QM/MM2 uses aliphatic parameters. There is overall a good agreement between the various description.

energy calculation of the system in T_1 from a single point energy calculation in the S_0. This is of course a very rough approximation within the chosen theoretical framework. Since the T_1 surface is believed to have a similar shape to the S_1, but lower in energy[9,10], utilizing ground state DFT on T_1 can be expected to introduce the error in the energy giving the largest deviation, and give too low excitation energies. The bandwidth, obtained from looking at the excitation energies of all the excitations, should not be as sensitive to this approximation, since the error introduced should be the same for each of the excitations.

Due to the limits set by the computational costs , an extrapolation to the excitation energies of each step in the entire GS trajectory is made, although no clear linear correlation between the Ir-Ir distance and excitation energy is observed. The complex is known to have an

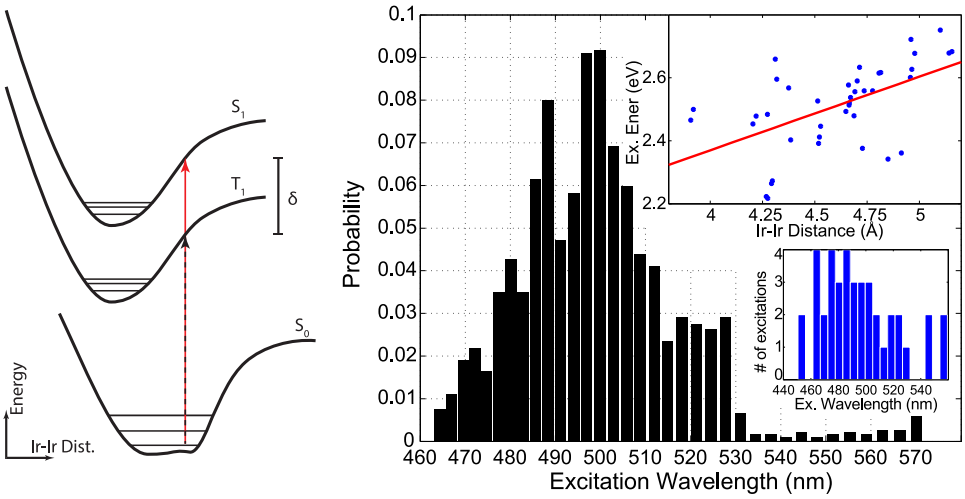

Figure 3: **Left:** Franck-Condon diagram sketching how the experimental excitation is approximated in the simulations, with δ being the error made from exciting to T_1 instead of S_1. **Right:** Approximation of the effective bandwidth used in creating the excited state population. The excitation energy is approximated by subtracting the single point energy of each initial GS configuration from a single point calculation of its ES spin configuration counterpart. The lower inset shows histogram of these energies, converted to wavelengths, and how many times they appear in the ES population. This is extrapolated to the entire GS trajectory, under the (crude) assumption that the excitation energy is linearly dependent on (and only on) the Ir-Ir distance, shown in the top inset. This relation is then used for obtaining the results shown in the main figure.

absorption maximum assigned to the long and eclipsed conformer at 475 nm[11], so it is expected due to the lower T_1 energy that the simulated excitation peak (fig. 3, left) is located

at lower energies. The experimental bandwith is 18.77 nm, and excitation wavelength is 477 nm[11]. The total effective bandwidth can be seen from the figure to be at least 100 nm, or 5 times the experimental bandwidth. Fig. 4 shows the Ir-Ir pinch in four subsets of the entire

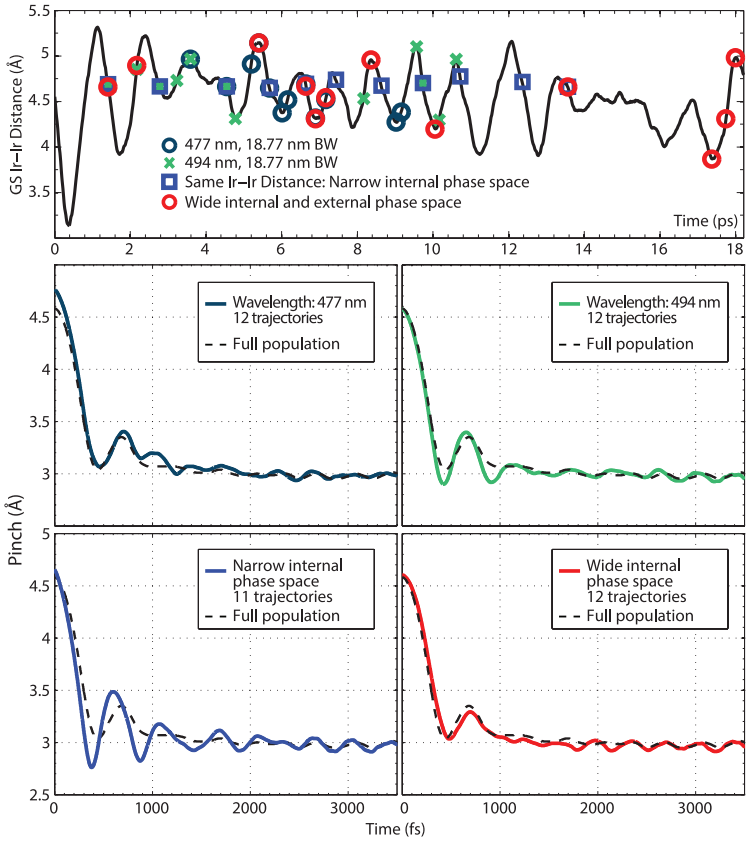

Figure 4: Splitting up the total ES population with respect to excitation energies, or by grouping initial configurations. The top two ES pinch graphs are made from selecting for ES trajectories with excitation energies assumed close to the experimental value and bandwidth. The bottom left subset is made from a narrow internal phase space of initial Ir-Ir distances. The last graph shows the dynamics of a wide phase space, but with the same statistics as the other three subsets.

phase space of the ES population. The top two are subsets of excitations with energies corresponding to wavelengths of 477 nm and 494 nm, respectively. The first having the same value as in the experiment, and the second is lower in energy to account for the error made in simulating the excitation energies. The bottom left subset is chosen to have the most narrow internal phase space possible, with identical initial Ir-Ir distances, but different solvent configurations. The last plot shows the pinch in a wide internal phase space, but

with similar sampling statistics, allowing for comparison of the four subsets.

As demonstrated in the lower right graph in 4, it is possible to obtain the same coherence-decay time using 12 trajectories as 40, which again means that any changes in coherence time in the other subsets are not simply due to worse statistics. Concentrating on the 477 nm and 494 nm excitation, the coherent pinch amplitude is observed to decay slightly slower than for the full population. Thus, the effective bandwidth in the simulation has, to some extent, an influence on the resulting coherent motion. Therefore, the incoherence in the initial ensemble is the main factor for the coherence decay of the ES population. This result is underpinned by the lower left graph, where the very narrow internal phase space greatly increases the coherence lifetime. This result is not surprising, since the GS pinch oscillation has a similar amplitude as the ES pinch.

References

(1) Jónsson, E. O.; Thygesen, K. S.; Ulstrup, J; Jacobsen, K. W. *Computational Approach to Electron Charge Transfer Reactions*; Technical University of Denmark: Lyngby, Denmark; 2014.

(2) Waldman, M.; Hagler, A. New Combining Rules for Rare Gas van der Waals Parameters. *J. Comput. Chem.* **2004**, *14*, 1077.

(3) Mortensen, J.; Hansen, L.; Jacobsen, K. W. Real-Space Grid Implementation of the Projector Augmented Wave Method). *Phys. Rev. B* **2005**, *71*, 035109.

(4) Haldrup, K.; Harlang, T.; Christensen, M.; Dohn, A.; van Driel, T. B.; Kjær, K. S.; Harrit, N.; Vibenholt, J.; Guerin, L.; Wulff, M. ; *et al.* Bond Shortening (1.4 Å) in the Singlet and Triplet Excited States of $[Ir_2(dimen)_4]^{2+}$ in Solution Determined by Time-Resolved X-Ray Scattering. *Inorg. Chem.* **2011**, *50*, 9329.

(5) Extrom, C. L.; Britton, D.; Mann, K. R. Structures of $[M_2(dimen)_4](Y)_2$ (M = Rh, Ir; dimen = 1,8-diisocyanomenthane; Y = PF_6, Tetrakis[3,5-

bis(trifluoromethyl)phenyl]borate, $B(C_6H_5)_4$) Crystals Featuring an Exceptionally Wide Range of Metal-Metal Distances and Dihedral Twist Angles. *Inorg. Chem.* **1996**, *35*, 549.

(6) Guardia, E.; Pinzón, R.; Casulleras, J.; Orozco, M.; Luque, F. J. Comparison of Different Three-Site Interaction Potentials for Liquid Acetonitrile. *Mol. Simulat.* **2001**, *26*, 287.

(7) Andersen, H. C. Rattle: A "Velocity" Version of the Shake Algorithm for Molecular Dynamics Calculations. *J. Comput. Phys.* **1983**, *52*.

(8) Petersen, J.; Henriksen, N. E.; Møller, K. B. Validity of the Bersohn–Zewail Model Beyond Justification. *Chem. Phys. Lett.* **2012**, *539-540*, 234–238.

(9) van der Veen, R. M.; Cannizzo, A.; van Mourik, F.; Vlcek, A. J.; Chergui, M. Vibrational Relaxation and Intersystem Crossing of Binuclear Metal Complexes in Solution. *J. Am. Chem. Soc.* **2011**, *113*, 305.

(10) Stiegman, A. E.; Rice, S. F.; Gray, H. B.; Miskowski, V. M. Electronic Spectroscopy of d^8-d^8 Diplatinum Complexes. $^1A_{2u}(d\sigma^* \rightarrow p\sigma)$, $^3E_u(d_{xz}, d_{yz} \rightarrow p\sigma)$, and $^{3,1}B_{2u}(d\sigma^* \rightarrow d_{x^2-y^2}$ Excited States of $Pt_2(P_2O_5H_2)_2^{4-}$. *Inorg. Chem.* **1987**, *26*, 1112.

(11) Hartsock, R. W.; Zhang, W.; Hill, M. G.; Sabat, B.; Gaffney, K. J. Characterizing the Deformational Isomers of Bimetallic $Ir_2(dimen)_4^{2+}$ (dimen= 1,8-diisocyno-*p*-menthane) with Vibrational Wavepacket Dynamics. *J. Phys. Chem. A* **2011**, *115*, 2920.